Reduction in field-aligned currents preceding and local to auroral substorm onset

Kyle R. Murphy,[1] Ian R. Mann,[1] I. Jonathan Rae,[1] Colin L. Waters,[2] Brian J. Anderson,[3] David K. Milling,[1] Howard J. Singer,[4] and Haje Korth[3]

Received 19 June 2012; accepted 4 July 2012; published 9 August 2012.

[1] We examine the global field-aligned current (FAC) topology associated with a clear substorm on the 16 February 2010. We show that for this particular substorm there is a clear and localised reduction in the FACs observed by AMPERE at least 6 minutes prior to auroral onset. A new auroral arc forms in the region of reduced FAC and on closed field lines which subsequently brightens and expands poleward, signifying the start of the substorm expansion phase. We argue that the change in FACs observed prior to onset is the result of a change in the magnetosphere-ionosphere (M-I) coupling in a region local to the subsequent auroral onset. Such a change implies an important role for M-I coupling in destabilising the near-Earth tail during magnetospheric substorms and perhaps more importantly in selecting the location in the ionosphere where auroral onset begins. **Citation:** Murphy, K. R., I. R. Mann, I. J. Rae, C. L. Waters, B. J. Anderson, D. K. Milling, H. J. Singer, and H. Korth (2012), Reduction in field-aligned currents preceding and local to auroral substorm onset, *Geophys. Res. Lett.*, *39*, L15106, doi:10.1029/2012GL052798.

1. Introduction

[2] Magnetic substorms are marked in the ionosphere by a well-defined sequence of events: a brightening of either the most equatorward growth-phase arc or a newly formed equatorward arc, the poleward motion of this arc and subsequent explosive break-up of the aurora [*Akasofu*, 1977, and references therein]. However, despite being well characterised in the ionosphere there is no consensus among researchers on the physical mechanism leading to the initiation of substorm onset in the magnetosphere (see, for instance, the debate in *Science* [*Angelopoulos et al.*, 2008; *Lui*, 2009; *Angelopoulos et al.*, 2009]).

[3] Two of the more commonly-debated substorm paradigms are the near-Earth neutral line (NENL) and current disruption (CD) models. Each of these phenomenological models describes a sequence of events in the magnetosphere which are suggested to directly relate magnetospheric phenomena to auroral activity in the ionosphere. In the NENL paradigm, magnetic reconnection initiates on stretched field lines at a distance of $\sim$20–25 R_E triggering magnetospheric substorm expansion phase onset [e.g., *Baker et al.*, 1996; *Angelopoulos et al.*, 2008]. In the CD paradigm magnetospheric expansion phase onset is triggered by a localised plasma instability in the inner magnetosphere [*Lui*, 1996], potentially by a ballooning mode [e.g., *Roux et al.*, 1991; *Samson et al.*, 1996], lower hybrid turbulence [e.g., *Huba et al.*, 1977], or a cross-field current instability in the central plasma sheet [e.g., *Lui et al.*, 1995; *Rae et al.*, 2010]. Other models including the near-Earth geophysical onset (NGO) [*Maynard et al.*, 1996] and global Alfvénic interaction [*Song and Lysak*, 2001] have also been postulated, although these latter scenarios typically receive less attention in the literature. Though each substorm paradigm hypothesises a link between the sequence of events in the magnetosphere and the well-defined sequence of auroral events observed in the ionosphere [*Akasofu*, 1964], the connection between the magnetosphere and ionosphere remains a critical element in all substorm models that is not well understood. In this paper we use detailed estimates of the field aligned currents (FACs) and ionospheric equivalent currents to show that there is a localised change in M-I coupling in advance of and in a region coincident with auroral onset.

2. Instrumentation

[4] We present the first in-situ observations of the structure and evolution of the FACs associated with a magnetic substorm from the Active Magnetosphere and Planetary Electrodynamics Response Experiment (AMPERE), together with supporting conjugate auroral images and ground-based and geosynchronous magnetometer data. The global FAC structure can be estimated with AMPERE using the vector magnetic field measured on the Iridium constellation of low-Earth orbiting satellites [*Anderson et al.*, 2000; *Waters et al.*, 2001]. Using the 66 Iridium satellites distributed in 6 orbital tracks, FACs can be determined on the scale of the MLT separation of the Iridium orbital planes at an altitude of $\sim$780 km. Reliable FAC estimates from AMPERE are derived when the system is quasi-stationary on the timescale of the satellite separation in each orbital track, $\sim$10 minutes so that temporal changes in the system between satellite passes can be neglected.

[5] Estimates of ionospheric equivalent current structures can be determined using a network of closely spaced ground-based magnetometers, to complement the AMPERE derived FACs. In this study, ground-based equivalent currents (ECs) are determined using the H- and D-component magnetometer data from the CARISMA [*Mann et al.*, 2008] and THEMIS [*Russell et al.*, 2008] magnetometer arrays. After a quiet day

[1]Department of Physics, University of Alberta, Edmonton, Alberta, Canada.
[2]School of Mathematical and Physical Sciences, University of Newcastle, Callaghan, New South Wales, Australia.
[3]Johns Hopkins University Applied Physics Laboratory, Laurel, Maryland, USA.
[4]NOAA Space Environment Center, Boulder, Colorado, USA.

Corresponding author: K. R. Murphy, Department of Physics, University of Alberta, Edmonton, AB T6G 2G7, Canada. (kmurphy@ualberta.ca)

0094-8276/12/2012GL052798

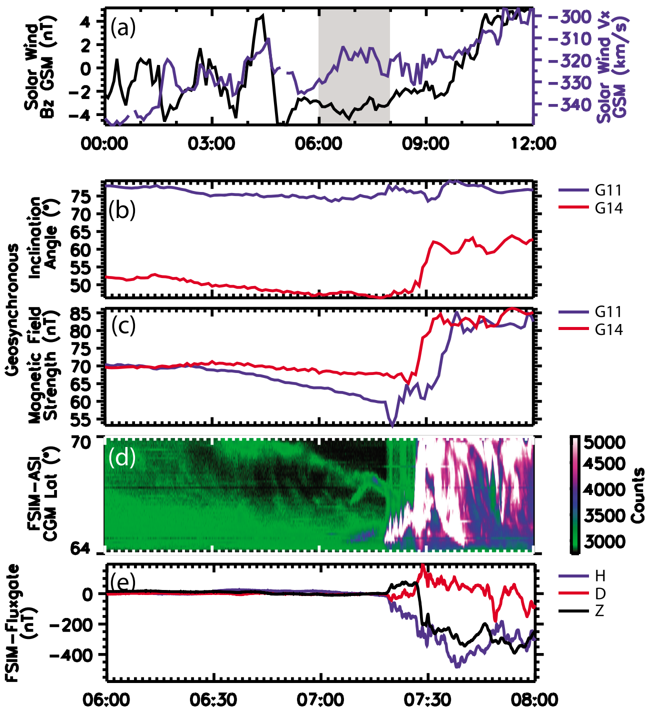

Figure 1. (a) The GSM x-component of the solar wind velocity (blue) and the GSM z-component of the solar wind magnetic field (black), the highlighted region denotes the time period during which the substorm is observed. (b) The G11 (blue) and G14 (red) inclination angle defined as the angle between the magnetic field and the vector sum of the x and y components in the local satellite ENP coordinate system. (c) G11 (blue) and G14 (red) total magnetic field strength. (d) FSIM ASI keogram; the keogram is constructed from a slice through the ASI perpendicular to the growth phase arc. (e) The H-, D-, and Z-component magnetic field variations from the FSIM magnetometer.

curve is removed from each magnetometer time series the entire dataset is interpolated onto a uniform grid and the ECs are calculated based on the infinite current sheet assumption [*Lühr and Schlegel*, 1994].

[6] In the following section we present a detailed picture of ground-based auroral and magnetic observations, as well as in-situ observations of the AMPERE FAC system and geosynchronous magnetic field perturbations during an isolated and very clearly characterised substorm observed on the 16 February 2010 between 06:00 and 08:00 UT. Auroral observations are provided by the THEMIS white light All-sky Imagers (ASIs) [*Mende et al.*, 2008] at a 3 second resolution and the NORSTAR Forth Smith (FSMI) meridian scanning photometer at 486 and 630 nm wavelengths (the proton and electron aurora, respectively) at a 30 second cadence [Donovan et al., 2003]. The geosynchronous magnetic field is provided by the GOES 11 and GOES 14 satellites (G11 and G14, respectively) at 60 second cadence [*Singer et al.*, 1996]. Higher resolution GOES 11 is not available for this event.

3. Observations: 16 February 2010

[7] Figure 1a shows the prevailing solar wind and IMF conditions propagated to the magnetosphere from the OMNI-2 database at 5 minute resolution [*King and Papitashvili*, 2005]. The highlighted region depicts the time period of interest during which the substorm is observed. During this period the GSM Bz is consistently small (mean of −3.4 nT) and directed southward and shows little variation and the solar wind velocity is relatively slow and constant (mean of −321 km/s). Figures 1b–1e show an overview of the substorm from 0600–0800 UT on the 16 February 2010 from geosynchronous orbit (Figures 1b and 1c) and from ground-based THEMIS Forth Simpson (FSIM) all-sky imager (Figure 1d) and CARISMA FSIM magnetometer (Figure 1e) at the location of auroral substorm onset. At onset G11 was located in the pre-midnight sector and conjugate to both the FSIM station and auroral onset and G14 was located around local midnight.

[8] A clear dipolarisation is observed at G11 and G14 at ∼07:25 UT, characterised by the sharp increase in the magnetic field strength and inclination angle observed at G14, typical of a magnetospheric substorm [*McPherron*, 1979]. Earlier there is a localised reduction in the G11 magnetic field strength of ∼5 nT for about 3 minutes around 07:19 UT–07:22 UT. A clear substorm growth phase is evident in the FSIM ASI keogram between ∼06:30–07:15 UT, characterised by the equatorward motion of the auroral oval [*Akasofu*, 1964]. Also apparent in the keogram is the formation of an equatorward arc at 07:06 UT which briefly fades and subsequently brightens and expands poleward at 07:18:30 UT marking auroral substorm onset [*Akasofu*, 1977]. This brightening and expansion is coincident in time with the reduction in magnetic field strength at the conjugate G11 satellite (to within the 60 s resolution of the GOES data). Auroral break-up at 07:25:30 UT is coincident in time with the dipolarisation at G14 and G11. Finally note the formation of the positive D-component and negative H- and Z-component magnetic bays at FSIM which are typical of the enhancement of ionospheric electrojets and formation of the substorm current wedge (SCW) following onset [*Clauer and McPherron*, 1974].

[9] Figure 2 shows the evolution of the aurora from the FSMI and FSIM ASIs and the FSMI MSP at selected times (see also the auroral animation in the auxiliary material).[1] The dotted blue line denotes the geomagnetic latitude of the peak in the proton auroral intensity at FSMI which marks the inner edge of the ion plasmasheet and the transition from dipole to tail-like magnetic field [*Samson et al.*, 1992]. The dotted red line marks the poleward border of the electron aurora at FSMI characterising the open closed field line boundary (OCFLB) in the magnetosphere [*Blanchard et al.*, 1995] determined using the method of *Rae et al.* [2004] (see Figure 2 caption). Both the peak in the proton aurora and poleward boundary of the electron aurora have been extended along lines of constant geomagnetic latitude to guide the eye and for reference to auroral forms in the FSIM ASI. At 07:17:30 UT (Figure 2a), the proton aurora reaches its minimum latitude, characteristic of the maximum stretching in the magnetotail and end of the growth phase. The yellow triangle marks the location of G11 traced magnetically to the northern hemisphere using T96 [*Tsyganenko*, 1995]. Figure 2b depicts auroral onset at 07:18:30 UT in the lower part of the FSIM ASI at 66° CGM latitude, which

[1]Auxiliary materials are available in the HTML. doi:10.1029/2012GL052798.

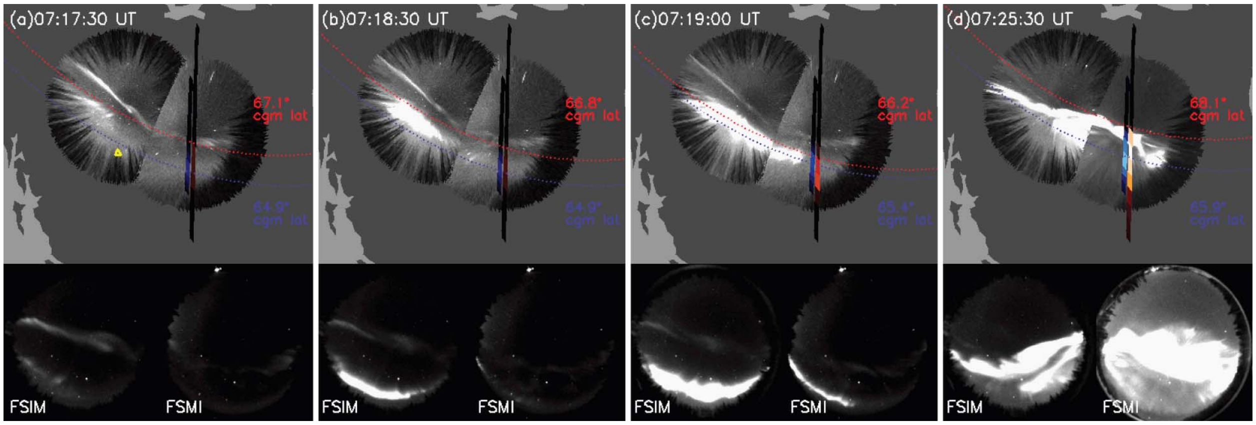

Figure 2. (a–d) Auroral dynamics between 07:17:30–07:25:30 UT as observed by the FSIM and FSMI ASI and FSMI MSP. (top) The mapped ASI data and the proton (blue) and electron (red) aurora from the FSMI MSP. The dotted blue line is a contour of constant CGM latitude at the peak in the proton aurora. The dotted red line marks the poleward edge of the electron aurora at constant CGM latitude. The poleward edge is determined by fitting the electron aurora intensity as a function of latitude to the functional form $f(x) = A_0 \exp\left(\frac{-1}{2} \times \left(\frac{x-A_1}{A_2}\right)^2\right)$. The poleward boarder is then defined as $A_1 + 1.5A_2$ [*Rae et al.*, 2004]. (bottom) The unmapped (left) FSIM and (right) FSMI ASI data. The yellow triangle in Figure 2a marks the T96 traced north magnetic foot print of G11.

corresponds to the first brightening of the equatorward arc clearly occurring on closed field lines equatorward of the OCFLB. Note that no poleward auroral streamers [*Nakamura et al.*, 2001] are seen within 6 hours of magnetic local time surrounding onset (also see the auroral animation in dissertation auxiliary material). Figure 2c shows the aurora at the time G11 observes a localised decrease in the magnetic field strength and Figure 2d depicts auroral breakup at 07:25:30 UT.

[10] Figure 3 shows the evolution of the FACs (red and blue shading) derived from AMPERE during available ten minute quasi-stationary periods and ground magnetometer

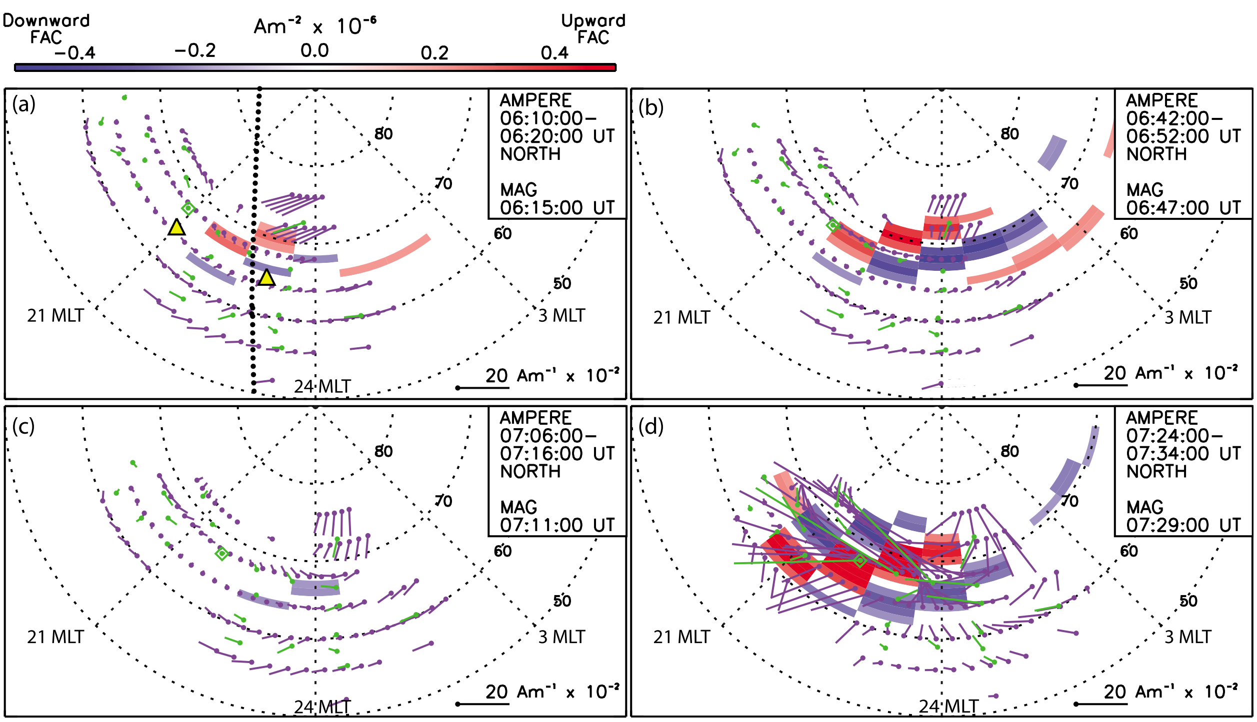

Figure 3. (a–d) The derived AMPERE FACs (red, upward and blue, downward) between 19 and 5 MLT during select ten minute quasi-stationary time periods and ground-based ECs at each station and interpolated onto a constant grid (green and purple, respectively) at the centre of each quasi-stationary period. The yellow triangles in Figure 3a mark the location of G11 (west) and G14 (east) and the black circles denote the trajectory of a single AMPERE orbital track in the pre-midnight sector (∼23 MLT). The green diamond in each panel marks the location of the FSIM ASI and magnetometer where auroral onset is observed.

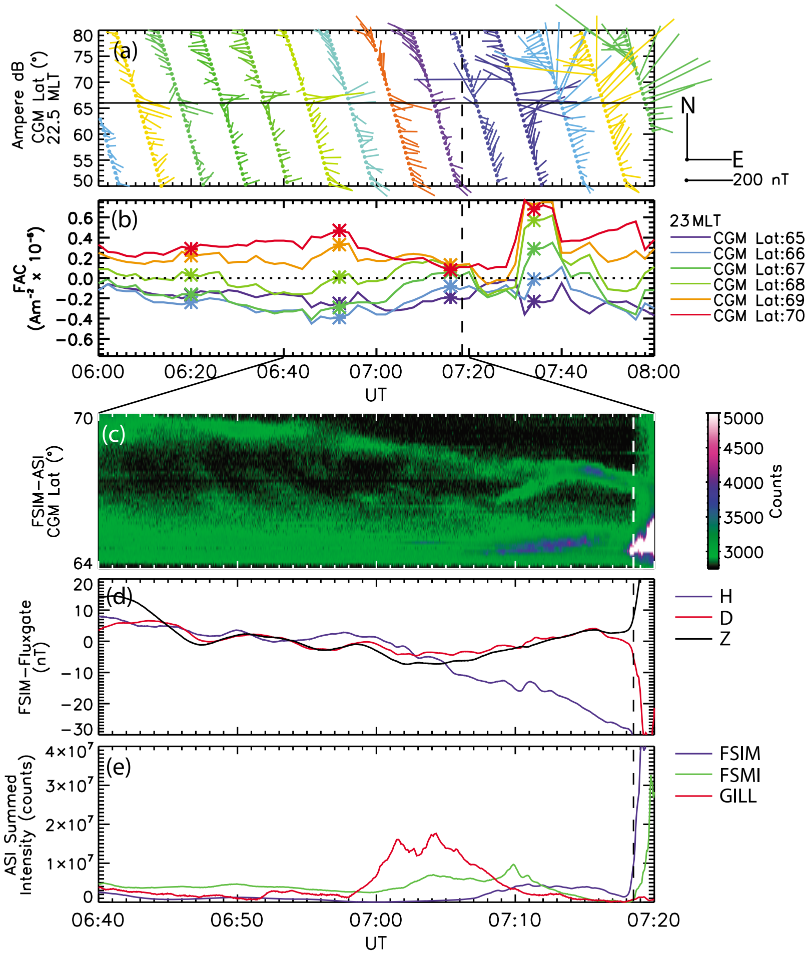

Figure 4. (a) The AMPERE geomagnetic N-S and E-W magnetic field perturbations at 1 minute resolution from the pre-midnight orbital track (cf. Figure 3a); the horizontal line marks the geomagnetic latitude of auroral onset at 66° CGM latitude. The vertical line in each panel marks auroral onset at 07:18:30 UT. (b) The AMPERE derived FACs in the auroral onset region at 23 MLT and from 65°–70° CGM latitude. (c) FSIM ASI keogram. (d) FSIM H-, D-, and Z-component magnetic field (blue, red and black respectively). (e) Integrated auroral intensity from select ASIs.

derived ionospheric ECs from each station, interpolated onto a regular grid (green and purple arrows respectively). A high latitude eastward electrojet in the dusk sector and lower latitude westward electrojet in the pre-midnight sector is apparent during the growth phase in Figure 3a in addition to an upward FAC system in the pre-midnight sector at ~70° CGM latitude and a downward FAC system just equatorward. As the growth phase progresses an enhancement in the eastward and westward electrojets [*McPherron et al.*, 1973] and upward and downward FACs are observed, (Figure 3b). Just prior to auroral onset, Figure 3c, a localised decrease in the ionospheric ECs and AMPERE FAC system is observed in a region coincident with the subsequent auroral onset (green diamond). The perpendicular ionospheric EC do not appear to change significantly in the nightside regions of the dawn and dusk convection cells. However, local to the subsequent onset region the perpendicular ground magnetic perturbations are smaller at this time. Finally, following auroral onset, Figure 3d shows a clear and strong enhancement of the ionospheric ECs and the development of a complicated system of upward and downward FAC sheets spanning from 20 MLT to 2 MLT. Although more complex in detail, this FAC structure is likely related to the SCW [*Murphy et al.*, 2011] and will be discussed in detail in a separate paper.

[11] Figure 4 is a stack plot of the AMPERE geomagnetic North-South (N-S) and East-West (E-W) magnetic field perturbations (Figure 4a) from the pre-midnight orbital track (dots in Figure 3a) that corresponds closely to the MLT of auroral onset, together with the derived FACs at 23 MLT (Figure 4b) the FSIM ASI keogram (Figure 4c) and magnetometer (Figure 4d) observations as well as the summed auroral intensity from the Gillam (GILL), FSMI and FSIM ASIs (Figure 4e). The dashed line at 07:18:30 UT and solid line at 66° mark the auroral onset time and geomagnetic latitude, respectively. A clear decrease in the magnetic field perturbations is evident in the pre-midnight AMPERE track at 07:12 UT at the latitude of auroral onset. Between 07:02–07:12 UT (the time between AMPERE passes) the distinctly eastward magnetic field feature between 63°–68° CGM latitude disappears. Similar to the pre-midnight AMPERE track the derived AMPERE FACs in Figure 4b show a clear decrease in the FAC strength prior to auroral onset. The asterisks in Figure 4b mark the end of the select quasi-

stationary 10 minute intervals shown in Figure 3, and the change in the FACs between these points is consistent with the overall conclusion that the FACs are reduced immediately prior to onset. Note in Figure 4b that large increases in the FACs following onset are only evident once the next AMPERE satellite along the 23 MLT track traverses the onset region, approximately ten minutes later. Evident in the ASI keogram and summed ASI intensities is the formation of an equatorward arc which propagates west (GILL to FSMI to FSIM) and dims at FSIM minutes prior to auroral onset. As the equatorward auroral arc forms at FSIM the observed magnetic field begins to diverge; a positive deflection is observed in the D- and Z-components and a negative deflection is seen in the H-component, consistent with a change in local field aligned and ionospheric currents. Interestingly, at the time of the arc dimming a second change in the magnetic field is seen in the FSIM magnetometer data, especially in the D- and Z-components.

[12] Two additional substorms observed on 24 March 2011 08:26:30 UT at the FSIM ASI and 16 May 2011 08:25:30 UT at The Pas ASI (see auxiliary material) also show a clear reduction in the AMPERE derived FACs in a region local to and preceding auroral onset. Significantly, the reduction in AMPERE FAC prior to auroral onset and at the same location suggests that there may be a role for M-I coupling in preconditioning the inner magnetosphere prior to auroral substorm onset.

4. Discussion and Conclusions

[13] In this paper, we present detailed observations of an isolated substorm event on 16 February 2010. A clear growth phase is marked by the equatorward propagation of the auroral oval and a clear and localised brightening of the aurora on the most equatorward arc is observed at 07:18:30 UT in the FSIM ASI denoting auroral substorm onset. This brightening occurs on closed field lines in the inner magnetosphere near the transition between dipole and tail field lines [*Samson et al.*, 1992] and coincident in time and closely conjugate with a decrease in the G11 geosynchronous magnetic field. No poleward auroral activations, such as the north-south auroral streamers described for example by *Nakamura et al.* [2001], are observed prior to this onset and thus there is no clear evidence in the THEMIS white light ASI data to suggest such distant magnetotail activity immediately precedes the auroral onset depicted in Figure 2b [cf. *Nishimura et al.*, 2010].

[14] However, there is a distinct change in the FACs observed by both AMPERE and ground-derived ionospheric ECs at the end of the substorm growth phase. The AMPERE FACs show a significant reduction in a region coincident with auroral onset and the pre-midnight AMPERE track shows a clear reduction in the N-S and E-W magnetic field perturbations between 07:06–07:12 UT. Coincident in both time and space with this FAC reduction is the formation and westward propagation of a newly formed equatorward arc. Shortly thereafter, the equatorward arc dims such that the intensity of the auroral emissions along the entire arc in the field of view of the FSIM camera is clearly reduced on the $\sim$1–2 minute time scales observed by *Pellinen and Heikkila* [1978]. Subsequently, the same arc then brightens and begins to move poleward at 07:18:30 UT characterising the beginning of the auroral onset in the same region which is precisely local to the prior reduction in FACs. During this entire period both the solar wind Bz and vx (GSM) remain nearly constant and the dayside FAC system (not shown) undergoes little change. Additionally, the westward electrojet continues to enhance for the entire duration of the growth phase. Thus it is unlikely that the change in the night-side FAC and ionospheric EC systems local to the auroral onset region occurs as the result of changes in large scale magnetospheric convection. More likely, there is a change in a localised region of the pre-midnight inner magnetotail which influences the processes leading to auroral substorm onset. We contend that the localised night-side reduction in FACs is the result of a change in magnetosphere-ionosphere coupling in a region conjugate to auroral onset. Determining how changes in magnetospheric and/or ionospheric processes and morphology lead to this FAC reduction and its potential role in the release of energy during onset is critical for understanding substorm onset.

[15] Localised reductions in the in-situ magnetic field are observed by AMPERE at least 6.5 minutes (and perhaps as long as 16.5 minutes) prior to auroral onset consistent with the reduction in FACs inferred by AMPERE during the same time period. This clearly demonstrates that there is a significant change in M-I coupling that precedes substorm onset. Certainly in this event, our observations clearly indicate that M-I coupling played a very significant role in the substorm onset process, perhaps by preconditioning the system prior to onset [cf. *Milan et al.*, 2010]. The exact role of this magnetosphere-ionosphere coupling process local to the onset remains to be determined. However, it is clear from these observations that any substorm model or paradigm must address the localised reduction in M-I coupling prior to onset within its framework. For example, perhaps the change in M-I coupling is responsible for the localised auroral dimming prior to onset [*Pellinen and Heikkila*, 1978] which subsequently leads to a destabilization of local near-Earth plasmasheet instabilities such as cross-tail current disruption [*Lui*, 1996] or ballooning at the edge of the equatorial plasma sheet [e.g., *Roux*, 1985; *Samson et al.*, 1996] leading to onset, or perhaps onset occurs as a result of the near-Earth geophysical onset (NGO) mechanism as described by *Maynard et al.* [1996]. The local reduction in magnetic field magnitude at onset seen at G11 may be very significant since it could be consistent with both the CD and NGO models as described for example by *Ohtani* [1998] and *Erickson et al.* [2000], respectively.

[16] The fact that the FAC reduction only occurs in a localised region, local to and 6.5 minutes before the subsequent auroral onset has important ramifications for the substorm paradigm. Our observations on 16 February 2010 (as well as those on 24 March 2011 and 16 May 2011 presented in the auxiliary material) clearly demonstrate the necessity of including the role of M-I coupling processes in the minutes preceding auroral onset in any substorm onset mechanism. Indeed these FAC changes could potentially be mediated via the exchange of Alfvén waves between the magnetosphere and ionosphere and therefore could represent a critical component of the onset process. In that case, not only would M-I coupling play a role in selecting the subsequent auroral onset location, but also the FAC could provide a basis for diagnosing the magnetospheric processes which must explain the well-known Akasofu sequence of auroral onset morphology in the ionosphere.

[17] **Acknowledgments.** K.R.M. is funded by an Alberta Innovates Graduate Scholarship. I.R.M. is supported by a Discovery Grant from NSERC. I.J.R. is funded by the Canadian Space Agency (CSA). We acknowledge NASA contract NAS5-02099 and V. Angelopoulos for use of data from the THEMIS Mission. Specifically, we thank S. Mende and E. Donovan for use of the THEMIS ASI data. The ground-based component of the THEMIS mission is funded by NSF award 1004736. Deployment and data retrieval of the THEMIS ASIs was partly supported by CSA contract 9F007-046101 to the University of Calgary. We thank S. Mende, Martin Connors and C. T. Russell for use of THEMIS ground-based magnetometer data. Alaska magnetometer data is provided courtesy of the Geophysical Institute Magnetometer Array operated by the Geophysical Institute, University of Alaska. More information about this dataset is available at http://magnet.asf.alaska.edu/. Operational support for NORSTAR is provided by the CSA and the University of Calgary. CARISMA is deployed and operated by the University of Alberta and funded by the CSA.

[18] The Editor thanks Anthony Lui and an anonymous reviewer for their assistance in evaluating this paper.

References

Akasofu, S. I. (1964), The development of the auroral substorm, *Planet. Space Sci.*, *12*, 273–282, doi:10.1016/0032-0633(64)90151-5.

Akasofu, S.-I. (1977), *Physics of Magnetospheric Substorms*, 274 pp., D. Reidel, Hingham, Mass., doi:10.1007/978-94-010-1164-8

Anderson, B. J., K. Takahashi, and B. A. Toth (2000), Sensing global Birkeland currents with Iridium® engineering magnetometer data, *Geophys. Res. Lett.*, *27*(24), 4045–4048, doi:10.1029/2000GL000094.

Angelopoulos, V., et al. (2008), Tail reconnection triggering substorm onset, *Science*, *321*(5891), 931–935, doi:10.1126/science.1160495.

Angelopoulos, V., et al. (2009), Response to comment on "Tail reconnection triggering substorm onset," *Science*, *324*(5933), 1391.

Baker, D. N., T. I. Pulkkinen, V. Angelopoulos, W. Baumjohann, and R. L. McPherron (1996), Neutral line model of substorms: Past results and present view, *J. Geophys. Res.*, *101*(A6), 12,975–13,010, doi:10.1029/95JA03753.

Blanchard, G. T., L. R. Lyons, J. C. Samson, and F. J. Rich (1995), Locating the polar cap boundary from observations of 6300 Å auroral emission, *J. Geophys. Res.*, *100*(A5), 7855–7862, doi:10.1029/94JA02631.

Clauer, R. C., and R. L. McPherron (1974), Mapping the local time–universal time development of magnetospheric substorms using mid latitude magnetic observations, *J. Geophys. Res.*, *79*, 2811–2820, doi:10.1029/JA079i019p02811.

Donovan, E. F., et al. (2003), All-sky imaging within the Canadian CANOPUS and NORSTAR projects, *Sodankyla Geophys. Obs. Publ.*, *92*, 109–112.

Erickson, G. M., N. C. Maynard, W. J. Burke, G. R. Wilson, and M. A. Heinemann (2000), Electromagnetics of substorm onsets in the near geosynchronous plasma sheet, *J. Geophys. Res.*, *105*(A11), 25,265–25,290, doi:10.1029/1999JA000424.

Huba, J. D., N. T. Gladd, and K. Papadopoulos (1977), The lower-hybrid-drift instability as a source of anomalous resistivity for magnetic field line reconnection, *Geophys. Res. Lett.*, *4*, 125–128, doi:10.1029/GL004i003p00125.

King, J. H., and N. E. Papitashvili (2005), Solar wind spatial scales in and comparisons of hourly Wind and ACE plasma and magnetic field data, *J. Geophys. Res.*, *110*, A02104, doi:10.1029/2004JA010649.

Lühr, H., and K. Schlegel (1994), Combined measurements of EISCAT and the EISCAT magnetometer cross to study Ω bands, *J. Geophys. Res.*, *99*(A5), 8951–8959, doi:10.1029/94JA00487.

Lui, A. T. Y. (1996), Current disruption in the Earth's magnetosphere: Observations and models, *J. Geophys. Res.*, *101*, 13,067–13,088, doi:10.1029/96JA00079.

Lui, A. T. Y. (2009), Comment on "Tail reconnection triggering substorm onset," *Science*, *324*(5933), 1391, doi:10.1126/science.1167726.

Lui, A. T. Y., C.-L. Chang, and P. H. Yoon (1995), Preliminary nonlocal analysis of cross-field current instability for substorm expansion onset, *J. Geophys. Res.*, *100*, 19,147–19,154, doi:10.1029/95JA01404.

Mann, I. R., et al. (2008), The Upgraded CARISMA magnetometer array in the THEMIS era, *Space Sci. Rev.*, *141*, 413–451, doi:10.1007/s11214-008-9457-6.

Maynard, N. C., W. J. Burke, E. M. Basinska, G. M. Erickson, W. J. Hughes, H. J. Singer, A. G. Yahnin, D. A. Hardy, and F. S. Mozer (1996), Dynamics of the inner magnetosphere near times of substorm onsets, *J. Geophys. Res.*, *101*(A4), 7705–7736, doi:10.1029/95JA03856.

McPherron, R. L. (1979), Magnetospheric substorms, *Rev. Geophys.*, *17*, 657–681, doi:10.1029/RG017i004p00657.

McPherron, R. L., C. T. Russell, M. G. Kivelson, and P. J. Coleman Jr. (1973), Substorms in space: The correlation between ground and satellite observations of the magnetic field, *Radio Sci.*, *8*(11), 1059–1076, doi:10.1029/RS008i011p01059.

Mende, S., et al. (2008), The THEMIS array of ground based observatories for the study of auroral substorms, *Space Sci. Rev.*, *141*, 357–387, doi:10.1007/s11214-008-9380-x.

Milan, S. E., A. Grocott, and B. Hubert (2010), A superposed epoch analysis of auroral evolution during substorms: Local time of onset region, *J. Geophys. Res.*, *115*, A00I04, doi:10.1029/2010JA015663.

Murphy, K. R., I. R. Mann, J. Rae, D. K. Milling, C. L. Waters, H. J. Singer, and B. J. Anderson. (2011), A multi-point and multi-instrument characterisation of the formation and evolution of the substorm current wedge, Abstract SM54A-04 presented at 2011 Fall Meeting, AGU, San Francisco, Calif., 5–9 Dec.

Nakamura, R., W. Baumjohann, R. Schödel, M. Brittnacher, V. A. Sergeev, M. Kubyshkina, T. Mukai, and K. Liou (2001), Earthward flow bursts, auroral streamers, and small expansions, *J. Geophys. Res.*, *106*(A6), 10,791–10,802, doi:10.1029/2000JA000306.

Nishimura, Y., L. Lyons, S. Zou, V. Angelopoulos, and S. Mende (2010), Substorm triggering by new plasma intrusion: THEMIS all-sky imager observations, *J. Geophys. Res.*, *115*, A07222, doi:10.1029/2009JA015166.

Ohtani, S. (1998), Earthward expansion of tail current disruption: Dual-satellite study, *J. Geophys. Res.*, *103*(A4), 6815–6825, doi:10.1029/98JA00013.

Pellinen, R. J., and W. J. Heikkila (1978), Observations of auroral fading before breakup, *J. Geophys. Res.*, *83*(A9), 4207–4217, doi:10.1029/JA083iA09p04207.

Rae, I. J., K. Kabin, R. Rankin, F. R. Fenrich, W. Liu, J. A. Wanliss, A. J. Ridley, T. I. Gombosi, and D. L. De Zeeuw (2004), Comparison of photometer and global MHD determination of the open-closed field line boundary, *J. Geophys. Res.*, *109*, A01204, doi:10.1029/2003JA009968.

Rae, I. J., C. E. J. Watt, I. R. Mann, K. R. Murphy, J. C. Samson, K. Kabin, and V. Angelopoulos (2010), Optical characterization of the growth and spatial structure of a substorm onset arc, *J. Geophys. Res.*, *115*, A10222, doi:10.1029/2010JA015376.

Roux, A. (1985), Generation of field-aligned current structures at substorm onsets, in *Proceedings of ESA Workshop on Future Missions in Solar, Heliospheric and Space Plasma Physics*, *Eur. Space Agency Spec. Publ.*, *ESA SP-235*, 151.

Roux, A., S. Perraut, P. Robert, A. Morane, A. Pedersen, A. Korth, G. Kremser, B. Aparicio, D. Rodgers, and R. Pellinen (1991), Plasma sheet instability related to the westward travelling surge, *J. Geophys. Res.*, *96*, 17,697–17,714, doi:10.1029/91JA01106.

Russell, C. T., et al. (2008), THEMIS ground-based magnetometers, *Space Sci. Rev.*, *141*, 389–412, doi:10.1007/s11214-008-9337-0.

Samson, J. C., L. R. Lyons, P. T. Newell, F. Creutzberg, and B. Xu (1992), Proton aurora and substorm intensifications, *Geophys. Res. Lett.*, *9*(21), 2167–2170, doi:10.1029/92GL02184.

Samson, J. C., et al. (1996), Substorm intensifications and resistive shear flow-ballooning instabilities in the near-Earth magnetotail, in *Proceedings of the Third International Conference on Substorms (ICS-3)*, *Eur. Space Agency Spec. Publ.*, *ESA SP-389*, 399.

Singer, H. J., et al. (1996), Monitoring space weather with the GOES magnetometers, *Proc. SPIE Int. Soc, Opt. Eng.*, *2812*, 299–308.

Song, Y., and R. L. Lysak (2001), Towards a new paradigm: From a quasisteady description to a dynamical description of the magnetosphere, *Space Sci. Rev.*, *95*, 273–292, doi:10.1023/A:1005288420253.

Tsyganenko, N. A. (1995), Modeling the Earth's magnetospheric magnetic field confined within a realistic magnetopause, *J. Geophys. Res.*, *100*(A4), 5599–5612, doi:10.1029/94JA03193.

Waters, C. L., B. J. Anderson, and K. Liou (2001), Estimation of global field aligned currents using the Iridium® system magnetometer data, *Geophys. Res. Lett.*, *28*(11), 2165–2168, doi:10.1029/2000GL012725.